Meteoritics & Planetary Science 36, 1377–1396 (2001)
Available online at http://www.uark.edu/meteor

Experimental simulation of atmospheric entry of micrometeorites

ALICE TOPPANI[1], GUY LIBOUREL[1,2], CÉCILE ENGRAND[3] AND MICHEL MAURETTE[3]

[1]CRPG-CNRS, BP20, F-54501 Vandœuvre-lès-Nancy, France
[2]ENSG-INPL, BP40, F-54501 Vandœuvre-lès-Nancy, France
[3]CSNSM, Bat. 104, F-91405 Orsay-Campus, France
*Correspondence author's e-mail address: toppani@crpg.cnrs-nancy.fr

(Received 2001 February 1; accepted in revised form 2001 July 10)

Abstract–Depending on their velocity, entry angle and mass, micrometeorites suffer different degrees of heating during their deceleration in the Earth's atmosphere, leading, in most cases, to significant textural, mineralogical and chemical modifications. One of these modifications is the formation of a magnetite shell around most micrometeorites, which until now could not be reproduced, neither theoretically nor experimentally. The present study was designed to better understand the entry heating effects on micrometeorites and especially the formation of the magnetite shell. Fragments of the Murchison and Orgueil meteorites were used as analogue material in flash-heating experiments performed in a high-temperature furnace; effects of temperature, heating duration, and oxygen fugacity were investigated.

These experiments were able to reproduce most of the micrometeorites textures, from the vesicular fine-grained micrometeorites to the totally melted cosmic spherules. For the first time, the formation of a magnetite shell could be observed on micrometeorite analogues. We suggest that the most plausible mechanism for the formation of this shell is a peripheral partial melting with subsequent magnetite crystallization at the surface of the micrometeorite. Furthermore, with this study, it is possible to estimate the atmospheric entry conditions of micrometeorites, such as the peak temperature and the duration of flash-heating.

INTRODUCTION

Micrometeorites are large interplanetary dust particles (IDPs) collected in deep-sea sediments (Brownlee, 1985) and in polar ice sheets (Maurette *et al.*, 1986, 1991a; Taylor *et al.*, 2000; Yada and Kojima, 2000). They dominate the amount of extraterrestrial material accreted by Earth with an estimated flux of ~40 000 tons per year (Love and Brownlee, 1993). These micrometeorites are in general related to the most primitive classes CI1, CM2 and CR2 carbonaceous chondrites (*e.g.*, Christophe Michel-Levy and Bourot-Denise, 1992; Kurat *et al.*, 1994; Gounelle, 2000) and are thought to originate either from comets or from asteroids (Hughes, 1978; Flynn, 1989). Their study may thus provide clues about the primitive solar system. However, the heating experienced by the micrometeorites during their deceleration through the Earth's atmosphere from kilometers per second to centimeters per second causes major changes to their textures, mineralogical and chemical compositions. A textural classification of micrometeorites based on the degree of heating reached during this atmospheric entry has been proposed (Kurat *et al.*, 1994). The micrometeorite types range from unmelted micrometeorites (fine-grained and crystalline), partially melted micrometeorites (scoriaceous micrometeorites) to completely melted micrometeorites (cosmic spherules). To identify the primary characteristics of the micrometeorites, it is therefore important to understand the mineralogical, textural and chemical modifications occurring during this atmospheric entry.

One of the major characteristic of micrometeorites is the occurrence of a thin magnetite shell surrounding most micrometeorites (Maurette *et al.*, 1991b; Kurat *et al.*, 1994; Engrand and Maurette, 1998; Genge *et al.*, 1997). In this paper, we prefer to name it "spinel rim" because the iron-rich phases of the rim belong to the spinel solid-solution (*e.g.*, Kurat *et al.*, 1994). Even though several scenarios of formation of this spinel rim have been proposed (Kurat *et al.*, 1994; Jessberger *et al.*, 1992; Maurette, 1998), its formation, thought to occur during atmospheric entry, is still poorly understood (Kurat *et al.*, 1994). This spinel rim formation had hitherto not been predicted by flash-heating modeling (*e.g.*, Bonny and Balageas, 1990) nor reproduced by laboratory experiments (Greshake *et al.*, 1998). Understanding spinel rim formation is however of interest for two main reasons. First, calculations (Flynn, 1989; Jackson and Zook, 1992) have shown that main-belt asteroidal particles have generally lower atmospheric entry velocities than cometary particles. This suggests that, for similar entry angles, cometary

Prelude preprint MS#4504

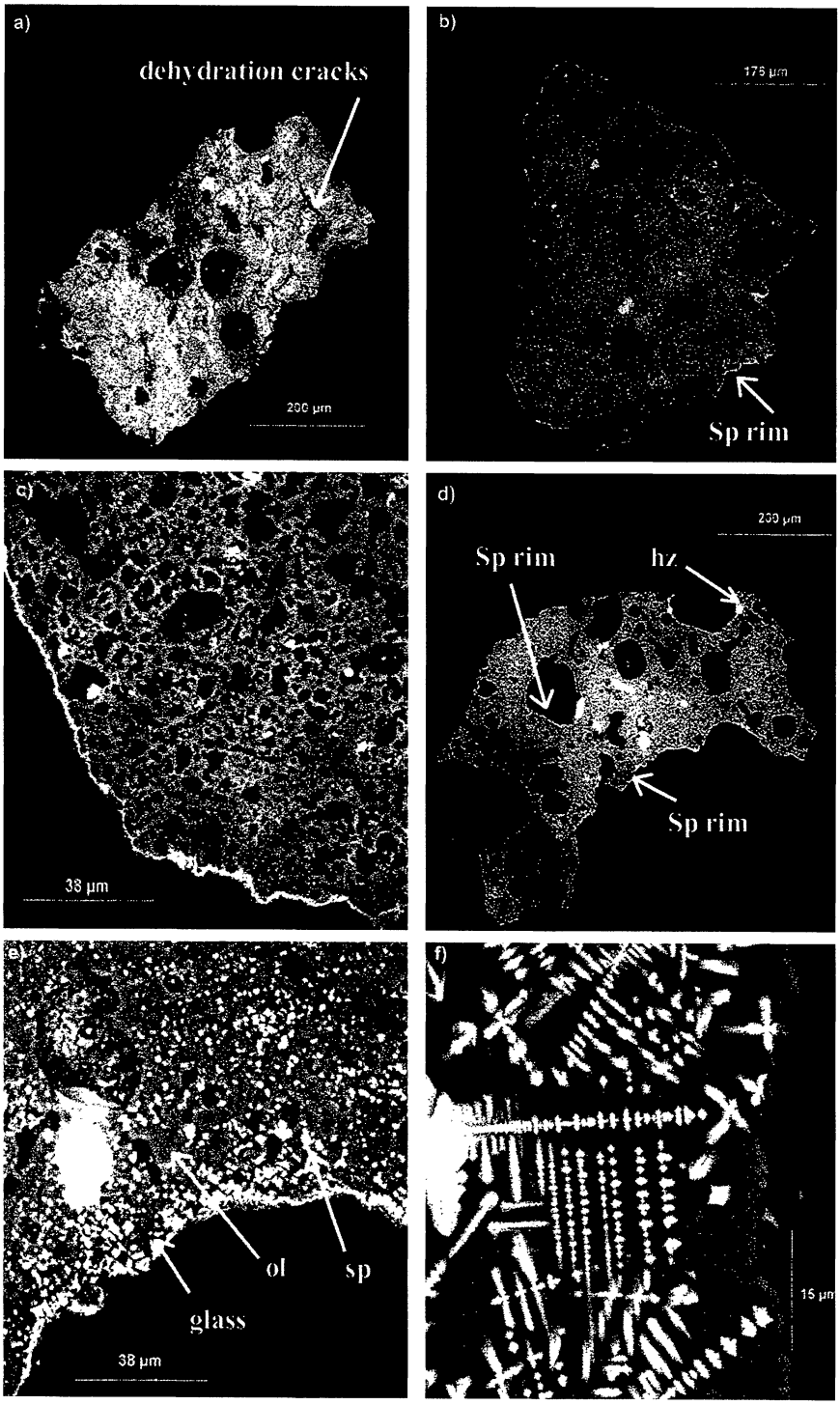

FIG. 1. Effect of the temperature on the textures of micrometeorite analogues during pulse-heating. Backscattered electron images of polished sections of Murchison fragments heated during 20 s, under an oxygen fugacity comprised between about –3 and about –4 log units at a temperature of (a) 1000 °C (run MM1000, see Table 1), (b) 1200 °C (run MM1200), (c) 1200 °C (detail of the edge of run MM 1200), (d) 1350 °C (run MM20), (e) 1350 °C (detail of the periphery of run 20), (f) 1500 °C (close-up view, run MM1500). The fragment heated at 1000 °C (a) shows evidence of dehydration in the form of cracks whereas fragments (b and c, d and e) show clear evidence for partial melting which progresses from the periphery to the core of the fragments with the crystallization of spinels and anhydrous silicates. The fragments heated at 1000 and 1200 °C (a, b, c) contain relic anhydrous silicates. The fragment heated at 1350 °C (d, e) has been completely reprocessed and shows numerous recrystallized anhydrous silicates (ol: olivine) and spinels. Some secondary sulfides (Ni_3S_2) are present at the periphery of this fragment (d) (hz: haezelwoodite). Fragments heated at 1200 and 1350 °C (b and c, d and e) are surrounded by a spinel rim (sp rim). Note that in the fragment heated at 1350 °C (d), some vesicles are also surrounding by a spinel rim. The last fragment (f) has been completely melted and shows dendritic spinels embedded in glass.

Starting Materials

Carbonaceous chondrite fragments were used as starting materials for these pulse-heating experiments. A first set of experiments was carried out using 200–400 μm sized fragments of Murchison, a CM2 carbonaceous chondrite (Fuchs *et al.*, 1973) as micrometeorite analogue because of the similarities between micrometeorites and CM2 chondrites (*e.g.*, Kurat *et al.*, 1994; Genge *et al.*, 1997; Engrand and Maurette, 1998; Gounelle, 2000). The unprocessed Murchison fragments (Fig. 1a) consist of an hydrous carbonaceous fine-grained matrix (~77%) hosting some larger isolated silicate grains such as olivines and Ca-poor pyroxenes, and rare chondrules (Fuchs *et al.*, 1973). The matrix is dominated by a Mg-Fe serpentine and tochilinite (*e.g.*, Barber, 1981).

Moreover, as unmelted micrometeorites are dominated by phyllosilicates, a second set of runs was carried out using chips of Orgueil as starting materials (see Fig. 2). Although the associations of phyllosilicates in unmelted micrometeorites can be different from those found in Orgueil (Noguchi and Nakamura, 2001), Orgueil offers the great advantage of consisting mainly of a fairly homogeneous matrix that can be used as a rather good analogue to fine-grained micrometeorites. Indeed, Orgueil matrix is rich in hydrated phases (*e.g.*, Böstrom and Fredriksson, 1966; Tomeoka and Buseck, 1988), and high-resolution transmission electron microscopy (TEM) studies of this matrix showed that two types of Fe-bearing, Mg-rich phyllosilicates occur within the matrix (Tomeoka and Buseck, 1988). The first type of phyllosilicate is very fine-grained and intergrown with S, Ni-rich ferrihydrite ($5Fe_2O_3\ 9H_2O$), which is also one important constituent mineral of micrometeorites. The coarse-grained phyllosilicate type occurs as 1 to 30 μm sized clusters. The ferrihydrite, intimately mixed with the phyllosilicates, represents ~60% of the iron content of the matrix (Tomeoka and Buseck, 1988). Magnetite is the second most abundant phase in CI chondrites and has been extensively studied (*e.g.*, Nagy and Claus, 1962; Hyman *et al.*, 1978; Hyman and Rowe, 1983). Its morphology is variable and includes magnetite framboids, spherulites and plaquettes (*e.g.*, Böstrom and Fredriksson, 1966; Jedwab, 1965, 1971; Kerridge, 1970; Hua and Buseck, 1998). Our magnetite analyses performed on unheated Orgueil fragments showed that the magnetites are pure Fe_3O_4, which is in agreement with the literature data (*e.g.*, Böstrom and Fredriksson, 1966; Folinsbee *et al.*, 1967; Kerridge, 1970).

Experimental Techniques

Experiments were performed at atmospheric pressure in a 1700 °C GERO HTVR 70-250 closed vertical furnace hosting an alumina muffle tube with a 4.2 cm inside diameter (CRPG-CNRS, Nancy). In the hot zone of the furnace, temperatures were measured with a $PtRh_{10}$-Pt thermocouple, calibrated against the melting temperature of silver, gold and palladium. Oxygen fugacity (fO_2) in each experiment was controlled by either CO_2-N_2 or CO_2-CO-N_2 gas mixtures, fed to the furnace at flow rates of 300 $cm^3\ min^{-1}$ using two or three Tylan mass flow controllers. The oxygen fugacity was controlled in the hotspot of the furnace using a fixed yttrium-stabilized zirconia probe before each experiment.

Pairs of 200 to 400 μm sized fragments of Murchison or Orgueil were selected and inserted into tiny crucibles made of spirals (4 mm length, 1.5 mm in diameter) of platinum wires (0.2 mm diameter) in order to enable the charge to react quickly with the gas flow. These spirals were attached to Pt baskets which were loaded into the hotspot of the furnace using an alumina rod equipped with a $PtRh_{10}$-Pt thermocouple. Because of the short duration of each experiment and the small size of the samples, the quench was performed in air by pulling out the sample holder from the hotspot to the top of the furnace. The experimental cooling rate is thus approximately constant between each experiment contrary to the slower cooling rates experienced by the micrometeorites during their deceleration in the Earth's atmosphere. The duration of pulse-heating includes the temperature rise time corresponding approximately to the time necessary to load the rod in the furnace (~1 s) added to the time at the peak temperature. In all experiments, the oxygen fugacity is established in the furnace prior to pulse-heating the sample. Air admitted in the furnace during the rapid entry of the sample at the beginning of the experiment is not taken into account for calculation of the fO_2 because of its very low amount.

Sample Preparation and Analytical Methods

Sample preparation was carried out at CSNSM in Orsay (France). After the heating experiments, samples were embedded in epoxy resin. Sections were polished with a reduced number of polishing steps, and in using only diamond paste. This allows us to avoid the rounding of the grain edge that would prevent the observation of the spinel rim on polished sections (Maurette, 1998).

Polished sections were studied in reflected light, and by backscattered electron (BSE) imaging with a SEM Hitachi S-2500 at the Université Henri Poincaré (Nancy, France). The mineralogical compositions were analyzed by the fully automated Cameca SX50 electron microprobe at the Université Henri Poincaré. An accelerating voltage of 15 kV, a beam current of 10 nA and a counting time of 30 s were used. Data were reduced by the ZAF method. Phase analyses were obtained with a focused beam while a defocused beam of 5 to 10 μm was used for profile analyses of bulk samples. One of the main difficulty encountered in the analysis of the spinels was the heterogeneity of the size of the crystals in many of our experimental runs, from 2 to 10 μm, which led to an enhancement of secondary fluorescence for the tiniest ones. Because data on small spinel crystals could contain a significant contribution of the silicate matrix, spinel analyses with $SiO_2 >$ 1 wt% were systematically discarded.

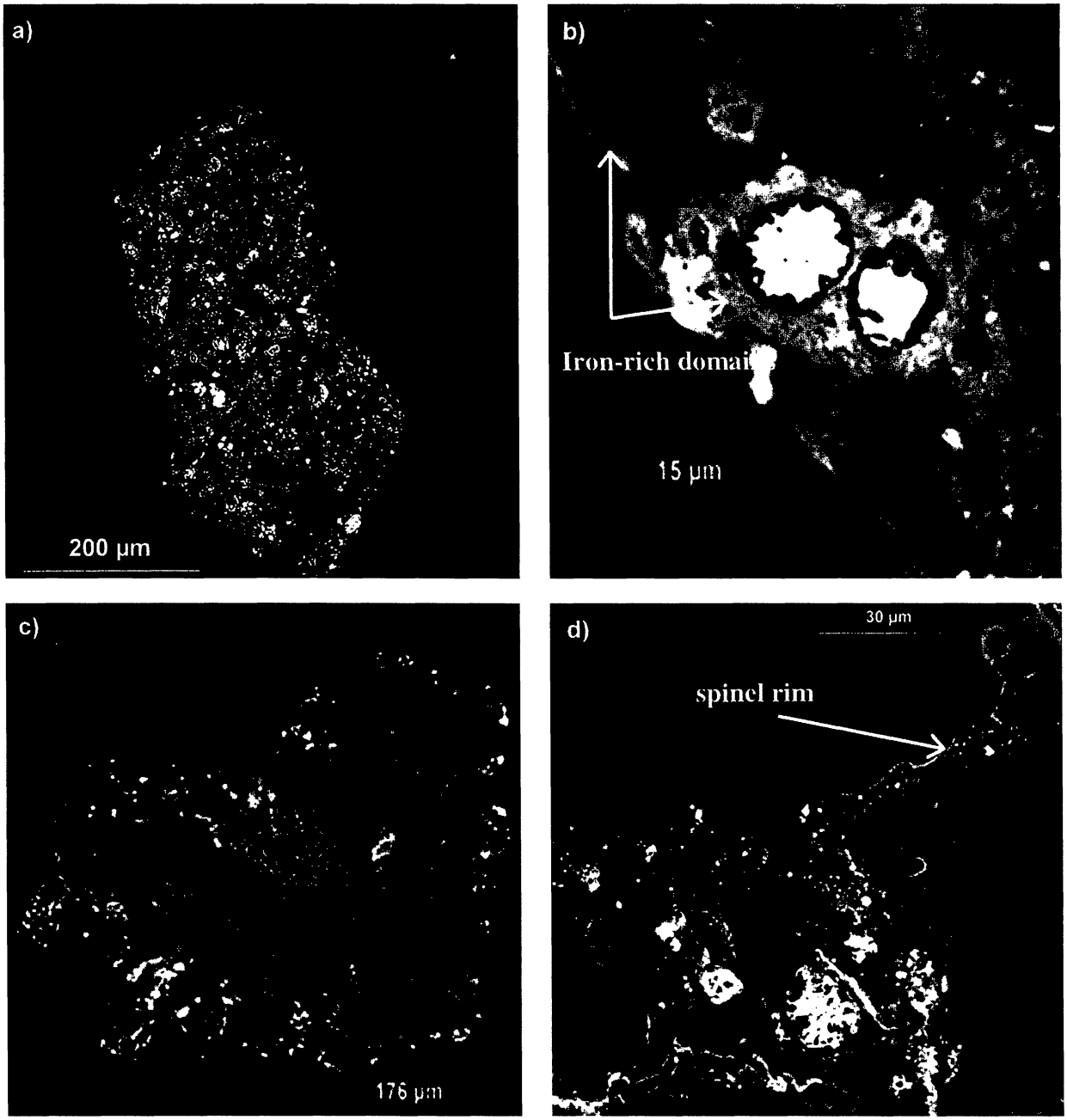

FIG. 2. Effect of the pulse-heating time on the textures of micrometeorite analogues at 1200 °C. Backscattered electron images of polished sections of Orgueil fragments heated at 1200 °C under $fO_2 = -0.68$ log units for: (a) 5 s (run 120/1/5); (b) 5 s (close-up view); (c) 20 s (run 120/1/20); (d) 20 s (close-up view). The first fragment (a, b) shows many dehydration cracks and evidence for destabilization of iron-rich phases. In (c) and (d), the fragment presents a higher rate of vesiculation and is surrounded by a thin spinel rim.

Iron Loss

When iron rich samples, such as Murchison or Orgueil fragments, are run in platinum holders, iron loss may occur and alter significantly the bulk composition (Corrigan and Gibb, 1979). However, we believe that the conditions of our experiments minimize this problem. Two adjacent fragments were put in each spiral to limit as much as possible contacts between sample and platinum holder. Furthermore, the short run duration (a few seconds to a few minutes) and the relative oxidizing conditions imposed in the runs (fO_2 ranging from –0.68 to –8 log units) allow only limited iron diffusion (Grove, 1981). Finally, the analyses of the platinum wires used in the run MM1500 (1500 °C, 20 s, $\log fO_2 = -3.6$) reveal that their

iron content is below the electron microprobe detection limits (FeO* ≈ 1000 ppm). However, for the longest run (120 s), care was taken by performing analyses on the heated samples far from the regions where the melted samples were in contact with the platinum wires.

RESULTS

The texture and mineralogical modifications will be described independently of the starting material, because Murchison and Orgueil samples show similar behavior. Changes in bulk and phase compositions will be reported only for the most homogeneous material (*i.e.*, Orgueil). All experimental conditions are listed in Table 1.

Texture

Effect of Temperature–In the following, we report results presenting the evolution of Murchison samples for heating pulses of 20 s in the range of 500 to 1500 °C.

TABLE 1. Experimental conditions.

Run	Meteorite	Temperature (°C)	Gas	$Log_{10}(fO_2)$	Duration (s)
MA500	Murchison	500	Air	–0.68	20
MM500	Murchison	500	96.5% CO_2 + 3.5% N_2	–8.12	20
MA1000	Murchison	1000	Air	–0.68	20
MM1000	Murchison	1000	96.5% CO_2 + 3.5% N_2	–4.92	20
MA1200*	Murchison	1200	Air	–0.68	20
MM1200*	Murchison	1200	96.5% CO_2 + 3.5% N_2	–3.88	20
MA5*, 10*, 20*, 40	Murchison	1350	Air	–0.68	5, 10, 20, 40
MM5*, 10*, 20*, 40	Murchison	1350	96.5% CO_2 + 3.5% N_2	–3.26	5, 10, 20, 40
MA1500	Murchison	1500	Air	–0.68	20
MM1500	Murchison	1500	96.5% CO_2 + 3.5% N_2	–2.76	20
50/1/20	Orgueil	500	Air	–0.68	20
50/2/20	Orgueil	500	96.5% CO_2 + 3.5% N_2	–8.12	20
80/1/20	Orgueil	800	Air	–0.68	20
100/1/20	Orgueil	1000	Air	–0.68	20
100/2/20	Orgueil	1000	96.5% CO_2 + 3.5% N_2	–4.92	20
120/1/5, 10, 20*, 40*, 120	Orgueil	1200	Air	–0.68	5, 10, 20, 40, 120
120/2/5, 10, 20*, 120*	Orgueil	1200	CO_2	–3.86	5, 10, 20, 120
120/3/40*, 120*	Orgueil	1200	99.6% CO_2 + 0.4% CO	–6.18	40, 120
135/1/5*, 10*, 20*, 40, 120	Orgueil	1350	Air	–0.68	5, 10, 20, 40, 120
135/2/5*, 10*, 20*, 40, 120	Orgueil	1350	96.5% CO_2 + 3.5% N_2	–3.26	5, 10, 20, 40, 120
135/3/5*, 20*, 40*, 120	Orgueil	1350	77.8% CO_2 + 20.2% N_2 + 2% CO	–5.96	5, 20, 40, 120
135/4/5*, 20*, 40*, 120*	Orgueil	1350	6.8% CO_2 + 91.2% N_2 + 2% CO	–8	5, 20, 40, 120
140/1/2*	Orgueil	1400	96.5% CO_2 + 3.5% N_2	–3.08	2
142/1/5*, 10, 20, 40, 120	Orgueil	1425	Air	–0.68	5, 10, 20, 40, 120
142/2/5*, 40, 120	Orgueil	1425	41.4% CO_2 + 58.6% N_2	–3.27	5, 40, 120
142/3/40, 120	Orgueil	1425	27% CO_2 + 71% N_2 + 2% CO	–6.08	40, 120
150/1/5, 120	Orgueil	1500	Air	–0.68	5, 120
150/2/5, 10, 120	Orgueil	1500	17.3% CO_2 + 82.7% N_2	–3.27	5, 10, 120
150/3/5, 120	Orgueil	1500	13.5% CO_2 + 84.5% N_2 + 2% CO	–5.96	5, 120

*Indicates the occurrence of a spinel rim around the pulse-heated samples.
Abbreviations: run 142/1/5 designates a run carried out at 1425 °C (142) under an oxygen fugacity of –0.68 log units (atmosphere of type 1) for 5 s (5). Atmospheres of type 1, 2, 3 correspond respectively to oxygen fugacity of about –0.68, –3.5, and –6 log units.

Pulse-heating at temperatures of 500 and 1000 °C (Fig. 1a) did not produce any significant textural evolution of the heated sample. Only an increased number of dehydration cracks are noticeable and shows a decrease of volume probably related to dehydration of the layer silicates. No polycrystalline spinel rim is formed. Samples pulse-heated at 1000 °C at highly oxidizing conditions (runs MA1000 and MM1000, see Table 1) had a reddish color, suggesting the presence of minute hematite crystals scattered in the fine-grained matrix and at the surface of the sample. This could be explained by the degradation of iron-rich phases into hematite (Cornell and Schwertmann, 1996).

As illustrated in Fig. 1b, major changes occur at 1200 °C. Abundant vesicles are scattered through the whole sample, with highly variable shapes (from angular to spherical) while their size may vary from a few micrometers to several tens of micrometers (Fig. 1c). Primary anhydrous silicates are still present and do not seem to be significantly affected by the heating, contrary to the constituent minerals of the matrix. The most noticeable feature is the 2–3 μm thick continuous, polycrystalline spinel rim surrounding the fragment. Only few crystals of spinel are observed inside the fragment (Fig. 1c).

The heated fragment at 1350 °C is characterized by a recrystallization texture, showing euhedral anhydrous silicates with occasional Fe/Mg zoning and abundant idiomorphous spinels embedded in a glassy mesostasis (Fig. 1d,e). The vesicles are less numerous, larger and more ovoid than in the sample heated at 1200 °C. Most of the vesicles are outlined by a thin spinel rim. This feature can also be observed on large primary anhydrous silicate grains located at the edge of the sample. The fragment is surrounded by a continuous spinel rim. Spinel crystals in the rim are on average bigger than those crystallizing toward the inner part of the fragment (Fig. 1e). Some Fe-poor sulfides, with a stoichiometry of haezelwoodite (Ni_3S_2), are also observed inside the fragment.

At temperature of 1500 °C, the fragment is completely melted with the occurrence of quench dentritic spinels and scarce anhydrous silicate crystals (Fig. 1f).

Thus, partial melting and recrystallization occurs during flash-heating above 1000 °C for 20 s, leading first to the crystallization of spinels around the sample and then toward the interior of the fragment in conjunction with that of anhydrous silicates.

Effect of Time–Time effects are here described by observation of Orgueil fragments heated during 5, 10, 20 and 40 s at temperatures of 1200 and 1350 °C under oxygen fugacities of –0.68 and –3.26 log units (Figs. 2 and 3).

At 1200 °C, fragments heated during 5 to 10 s do not show any spinel rim, nor recrystallized spinels. A few dehydration cracks are observable within the fragment. Figure 2a,b reveal that primary magnetite and iron-rich phases such as ferrihydrite seem to be destabilized leading to iron-rich domains. These iron-rich domains are more numerous along the cracks and around the fragment very likely due to a preferential dehydration. For a run duration of 20 s, the heterogeneous distribution of iron is less noticeable and a thin polycrystalline spinel rim (1–2 μm) is observed (Fig. 2c,d). For a run duration of 40 s (not shown here), vesiculation and spinel rim thickness slightly increase. Spinel crystals begin to crystallize inward the fragment as partial melting progresses.

At 1350 °C, for a run duration of 5 s, the fragment shows numerous ovoid vesicles of different sizes with an increase in the vesicle density near the edge of the sample (Fig. 3a,b). A clear 2 μm rim of spinel is observable at the sample's periphery. Minute spinels are also found in the first 30 μm of the fragment below the spinel rim.

For duration runs from 10 to 20 s, partial melting of the fragments is more noticeable than for run duration of 5 s with small spinel crystals beginning to crystallize toward the core of the chip together with euhedral anhydrous silicates (Fig. 3d). The vesiculation of the fragment becomes more significant, as shown in Fig. 3c, with a net increase of the size and the sphericity of the vesicles. Hence, the comparison between Fig. 3b and Fig. 3d suggests that the sphericity of the vesicles is strongly related to the rate of partial melting of the samples. A spinel rim surrounds each sample and some of the vesicles. The euhedral spinel crystals at the rim of the sample are larger (1.5 to 6 μm) than for the run time of 5 s.

For a 40 s heating time, the recrystallization texture is more homogeneous with anhydrous silicates and spinels clearly embedded in glass (Fig. 3e). The spinel rim is less continuous than for shorter duration run.

For longer run times (120 s), the texture is homogeneous (Fig. 3f) with larger recrystallized zoned anhydrous silicates and spinels. Spinel crystals are generally smaller and more dispersed inside the fragment. Furthermore, the spinel rim has completely disappeared.

Secondary electron images of the external surface of unpolished Orgueil fragments heated at 1350 °C under log $fO_2 = -8$ for run times between 5 to 20 s reveal that spinel crystals stand out of the melt. Furthermore, for short times (Fig. 4a), spinels are small (<1 μm) and very numerous, allowing a complete coverage of the sample's surface. For longer run time (Fig. 4b), the spinel crystals are larger (~1.5 μm) and less abundant, with the occurrence of melt between the crystals. These observations are in agreement with those performed on polished thin sections of heated Orgueil fragments.

These results show that the spinel rim forms over a restrictive range of run times from seconds to few tens of seconds. Its formation and characteristics, dependant on the rate of partial melting, are thus strongly controlled by the intensity and the length of the pulse-heating.

Effect of Oxygen Fugacity–The effects of oxygen fugacity are illustrated here by Orgueil samples run at fixed temperature and time (1350 °C, 5 s) under various oxygen partial pressures (fO_2 from –0.68 to –8 log units). In general, a decrease of the oxygen fugacity leads to a significant decrease in the abundance of spinel in the sample, as shown for example in Fig. 5a,b. It can also be seen that the thickness of the spinel rim (from 3–4 to 1–2 μm), the average size of spinel crystals and the scattering

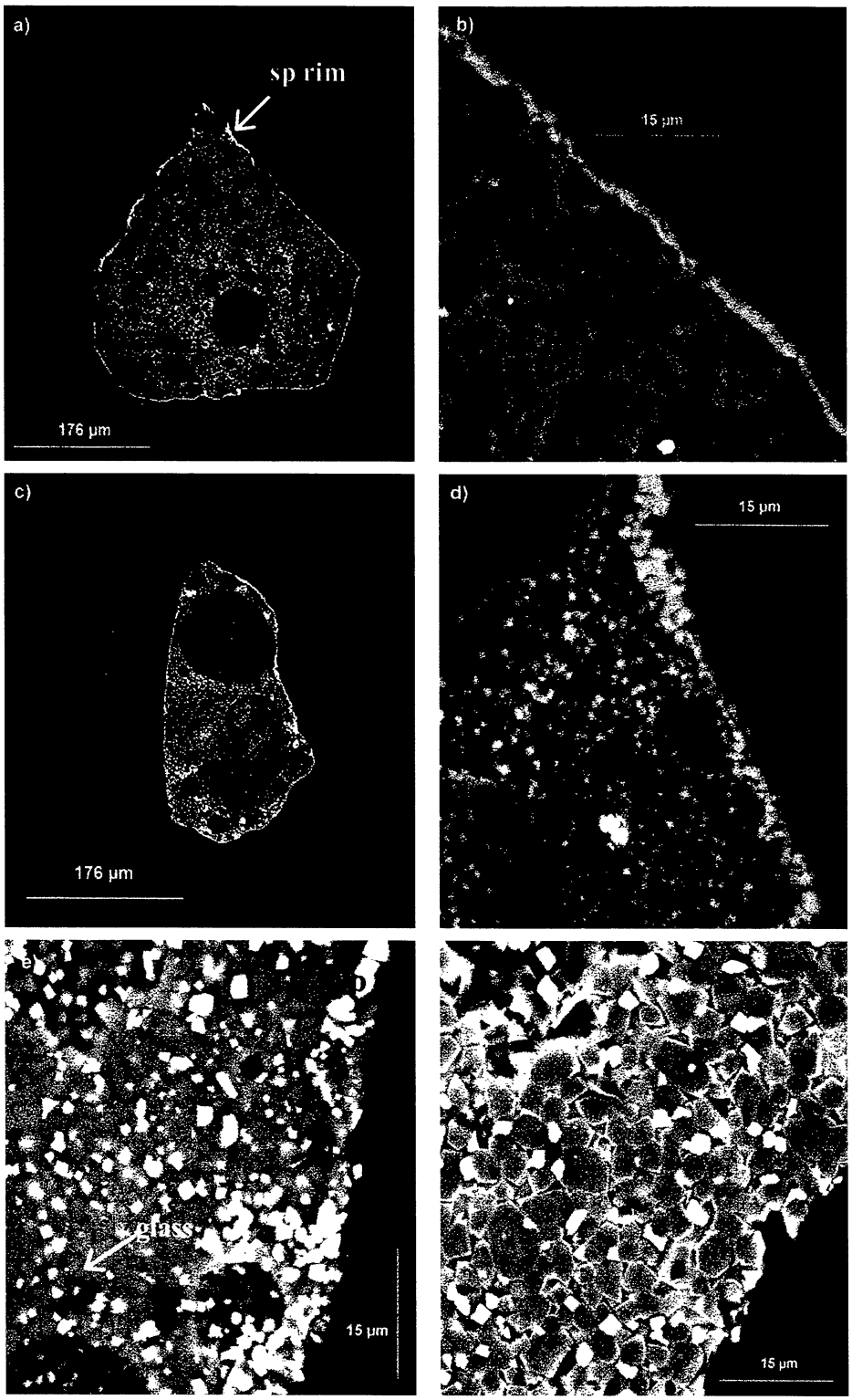

FIG. 3. Effect of the pulse-heating time on the textures of micrometeorite analogues at 1350 °C. Backscattered electron images of polished sections of Orgueil fragments heated at 1350 °C, under $fO_2 = -3.26$ log units for: (a) 5 s (run 135/2/5), (b) 5 s (close-up view), (c) 10 s (run 135/2/10), (d) 10 s (close-up view), (e) 40 s (run 135/2/40), (f) 120 s, under $\log fO_2 = -5.96$ (run 135/3/120). Note that in the first fragment (a, b), spinel occurs only at the periphery whereas in the second fragment (c, d) spinel begins to crystallize inward. In pictures (e, f), the homogenization of the texture leads to the disappearance of the spinel rim. The longer run time (f) has led to the growth of secondary anhydrous silicates and to dispersion of spinels within the fragment.

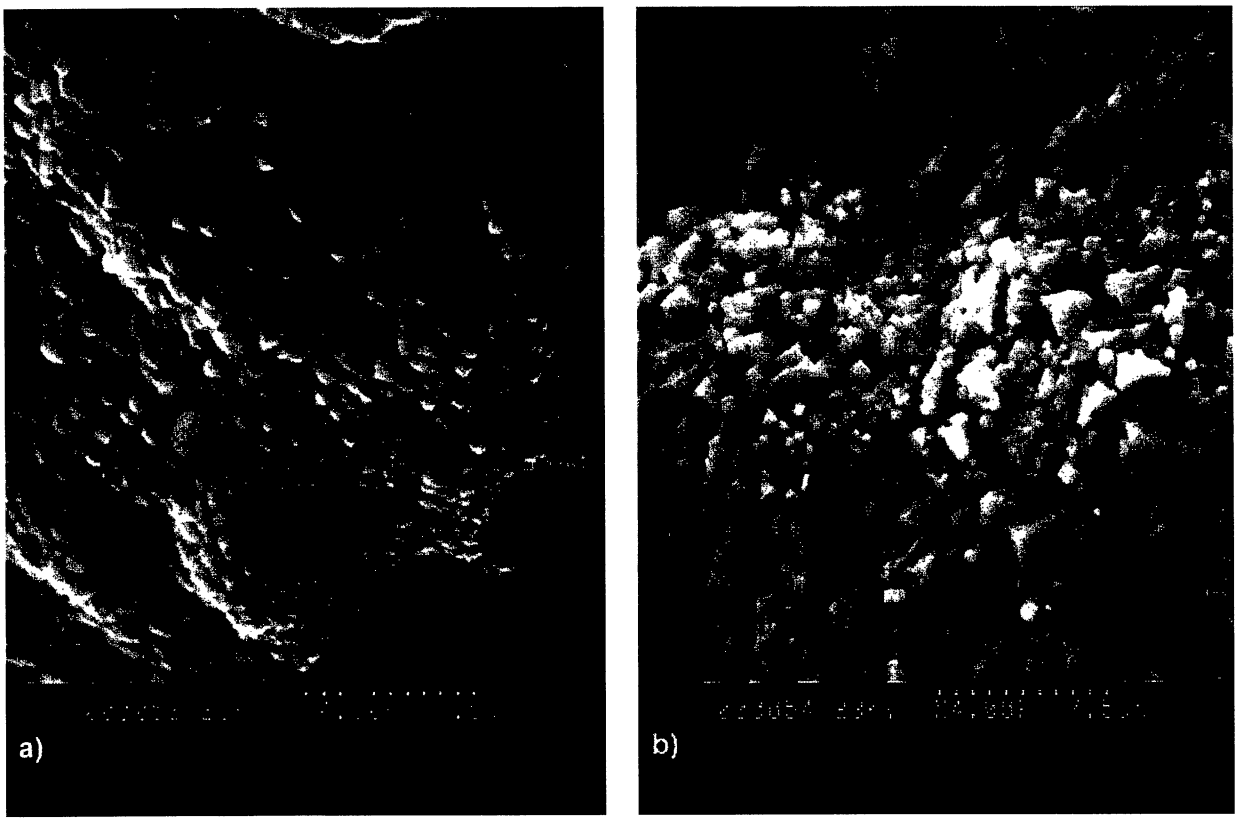

FIG. 4. Secondary electron images of the surface of Orgueil fragments heated at 1350 °C under $\log fO_2 = -3.26$ for: (a) 5 s (run 135/2/5), (b) 20 s (run 135/2/20). The longer the heating times, the larger and the less abundant are the spinel crystals at the surface of the fragment. On the second micrograph (b), glass can be seen between the crystals, showing that spinels crystallize from a melt. Note that spinel crystals stand out of the particle.

of spinel crystals near the edge of the sample all decrease by lowering the fO_2. The sample vesiculation as a function of the oxygen fugacity was more difficult to comprehend. However, for samples run at the highest temperature of 1500 °C, an increase in oxygen fugacity leads to a net increase in the degree of vesiculation of the sample (Fig. 5c,d), presumably due to a higher volatilization rate at high oxygen fugacity.

Effect of Starting Composition–Changes of texture and mineralogy as a function of temperature, flash-heating time and oxygen fugacity are approximately similar for both Murchison and Orgueil starting materials. However, a few differences have been noted (Fig. 6). Orgueil is more vesiculated than Murchison. This could be very likely due to the higher amount of volatile elements in Orgueil (Jarosewich, 1990). For long heating pulses (20 to 40 s) performed at a fixed oxygen fugacity, the modal abundance of spinels in Murchison samples seems to be higher than in Orgueil, in agreement with the higher iron concentration of the Murchison matrix composition (McSween and Richardson, 1977).

Chemical Compositions

Electron microprobe profiles using broad beam conditions were used to characterize the changes in the bulk compositions of pulse heated fragments of Orgueil.

Figure 7a shows the bulk composition of Orgueil fragments heated at 1350 °C under $fO_2 = -5.96$ log units for different run times. Figure 7b shows the bulk composition of Orgueil fragments heated under similar fO_2 during 10 s at temperatures of 1200 and 1350 °C, respectively. Bulk compositions are normalized to the Orgueil matrix composition (McSween and Richardson, 1977). The starting material's heterogeneity taken into account, there is no systematic chemical fractionation due to an increase of the temperature or of the duration of the pulse-heating, except for sulfur. Indeed, the sulfur content of micrometeorite analogues decreases with heating time and reaches very low values for the longest run time of 120 s (Fig. 7a). Similarly, the sulfur content decreases with temperature. Our results on the effects of time and temperature on the S content during simulated flash heating are thus compatible with those obtained by Greshake *et al.* (1998).

Profiles have been obtained across Orgueil fragments heated at the low temperature of 800 °C during 20 s in air and at the high temperatures of 1200 and 1350 °C under $fO_2 = -0.68$ and –3.26 log units, respectively, for different run times. No systematic variations are observed for the major elements within the samples except for sulfur and for tiny perturbations in Fe, Mg and Si due to spinel precipitation at the edge of the sample. For sulfur, Fig. 8 indicates that (1) fragments heated for short

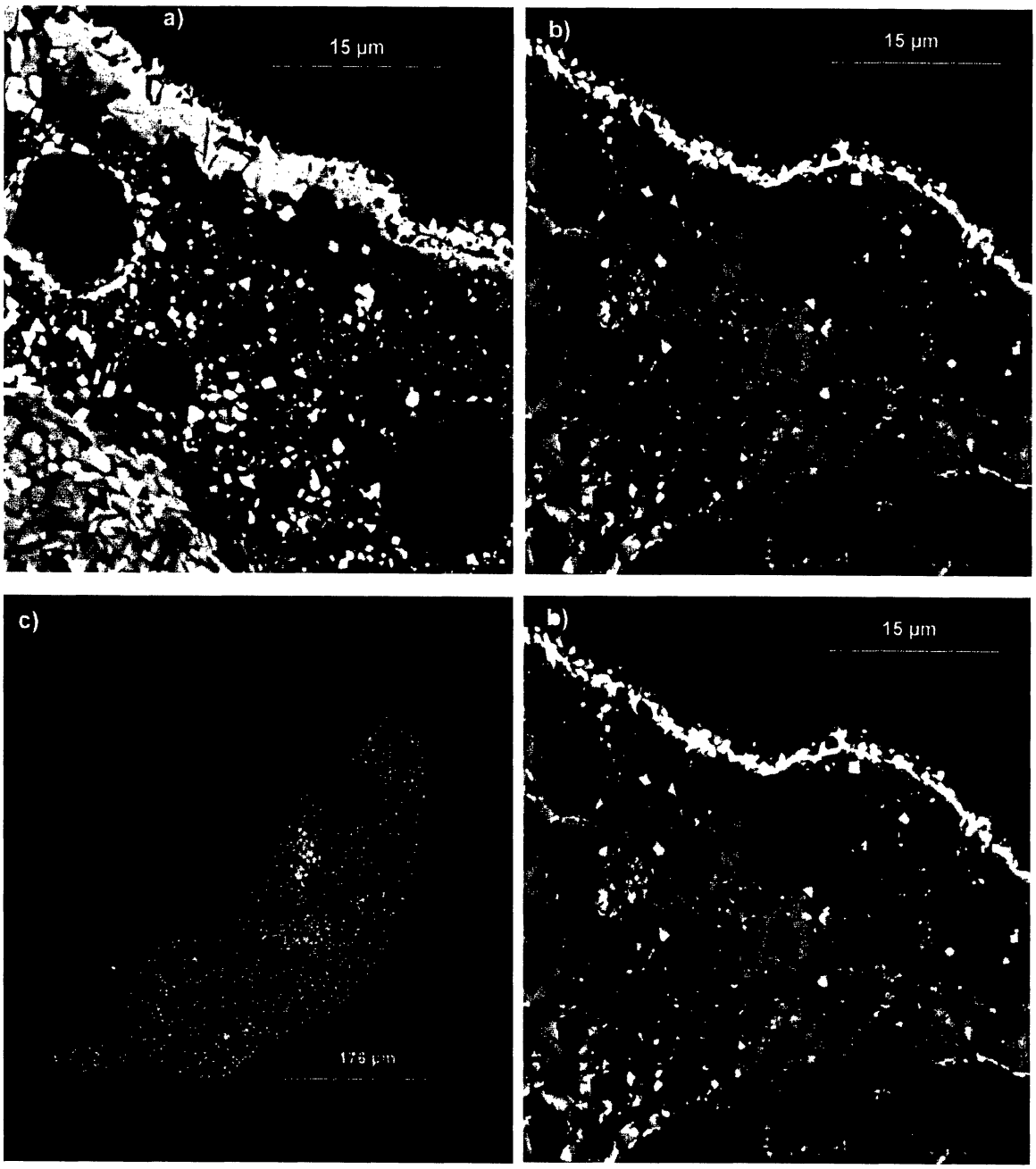

FIG. 5. Backscattered electron images of polished sections of Orgueil fragments heated at 1350 °C for 20 s, under (a) $fO_2 = -0.68$ log units (run 135/1/20) and (b) –5.96 log units (run 135/3/20) illustrating the influence of fO_2 on spinel occurrence. Note the decrease of size and abundance of spinel as fO_2 decreases. The effect of fO_2 on vesiculation rate is illustrated by the electron micrographs of polished sections of Orgueil fragments heated at 1500 °C, for 5 s under (c) $fO_2 = -0.68$ log units (run 150/1/5) and (d) –5.96 log units (run 150/3/5).

times and low temperatures show primary heterogeneity in the core with a depletion at the very edge; (2) at high temperature, the sulfur content is depleted throughout the whole sample by a factor of ~2 compared to a low-temperature heating at 800 °C; (3) at these high temperatures, the shape of the sulfur profile is related to the duration of the heating-pulse. This gradient in the fragments heated at higher temperatures might relate to diffusion in the more homogeneous melted particles. For instance, heating at 1200 °C for 10 s does not affect the shape of the profile, although for 20 s run time, a gradient exists in the sulfur content from the core to the border of the fragment. Longer run times lead to a flatter and lower sulfur content through the whole fragment (Fig. 8, run time of 40 s).

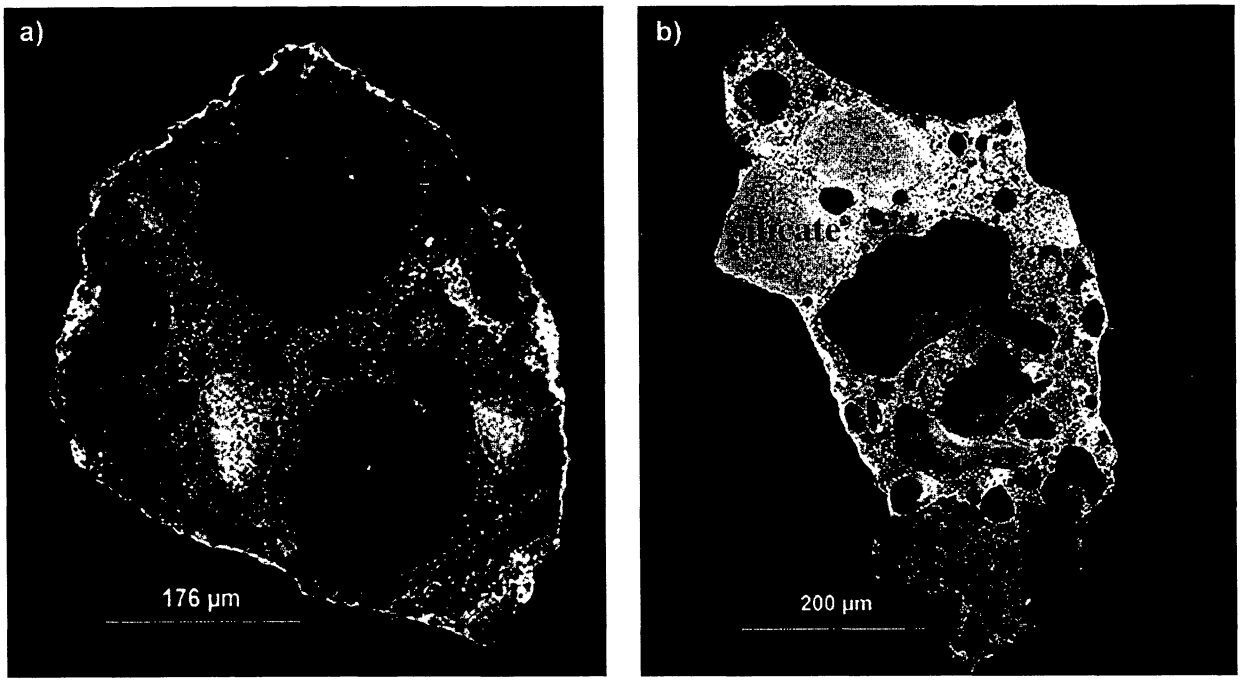

FIG. 6. Backscattered electron images of polished sections of (a) Orgueil (run 135/1/20) and (b) Murchison fragments (run MA20) heated in the same conditions (at 1350 °C for 20 s in air), showing the influence of the starting composition on the texture. Note that vesiculation in the Orgueil fragment is more developed than in the Murchison fragment and that spinel is more abundant inside the heated Murchison fragment than in the Orgueil fragment. Note also the heterogeneity of the Murchison fragment, with the presence of (1) two large anhydrous silicates at the top of the fragment and (2) a fragment of a chondrule (ch) at the bottom of the figure. The chondrule consists mainly of anhydrous silicates and chromite in a glassy mesostasis. Both the Orgueil and the Murchison fragments are encapsulated in a spinel rim.

Mineralogical Composition

The partial-melted zones at the periphery of the heated samples are constituted by a simple mineralogy of spinels, anhydrous silicates and glass. Table 2 presents spinel compositions probed in samples heated at 1350 °C in air for different run times and some anhydrous silicate and glass analyses obtained for long run times (40 s).

Spinels–Spinel compositions, determined by electron microprobe, show variable amounts of MgO (8–11 wt%), Al_2O_3 (0–2 wt%) and NiO (0.5–3 wt%). In contrast to terrestrial spinels (Haggerty, 1976), they contain high amounts of NiO and a low Fe^{2+}/Fe^{3+} ratio (between 0.15 and 0.25) showing a relatively high iron oxidation state for these spinels. In terms of end-members, these spinels correspond to the magnetite (Fe_3O_4)—magnesioferrite ($MgFe_2O_4$) solid-solution with variable amount of trevorite ($NiFe_2O_4$) and spinel *sensu-stricto* ($MgAl_2O_4$). The spinel compositions (see Table 2) reveal that concentrations of Mg, Ni, Al increase with heating time. For the longest times, spinels seem to reach a compositional plateau with minor variations in their Mg, Al or Ni contents, indicative of conditions approaching equilibrium. This is supported by the decrease in the chemical heterogeneity of spinels with time, as shown by the decrease in the standard deviation calculated from the electron microprobe analyses. Zoned spinels with a chromiferous core (up to 50 wt% Cr_2O_3) were usually observed in charges heated for long run times.

Anhydrous Silicates and Melt–For long duration runs, spinels and anhydrous silicates are usually embedded within a Fe-rich glassy mesostasis, as illustrated by analyses of Table 2. With up to 23 wt% FeO, this melt is highly enriched in iron by comparison with terrestrial rocks (<20 wt% FeO; Brooks *et al.*, 1991) and is expected to be even richer in iron for the shortest run times. The recrystallized anhydrous silicates are mainly constituted by olivines with variable iron contents. Partitioning coefficients calculated from a representative melt and recrystallized olivine or spinel compositions for long duration runs (*e.g.*, $D_{Ni}^{ol\text{-}liq} \approx 16$ and $D_{Ni}^{mt\text{-}liq} \approx 20$) are consistent with a crystallization from a silicate melt (Beattie *et al.*, 1991; Nielsen *et al.*, 1994).

COMPARISON WITH MICROMETEORITES

Cosmic Spherules

A convincing resemblance exists between the stony cosmic spherules and our completely melted charges (see Table 1, runs

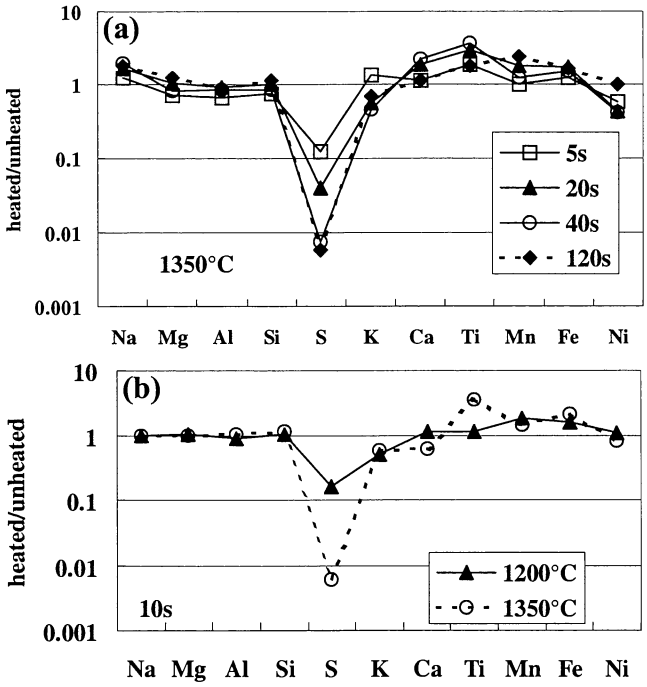

FIG. 7. Concentrations of major and minor elements in heated Orgueil fragments relative to unheated Orgueil fragment (data from McSween and Richardson, 1977), except for Ca which is normalized to our Orgueil fragments): (a) temperature of 1350 °C under $\log fO_2 = -5.96$ for different heating times (runs 135/3/5, 20, 40, 120); (b) heating for 10 s under $\log fO_2 \approx -3.5$ for different temperatures (runs 120/2/10 and 135/2/10).

150/2/5 or 135/1/40 and compare Figs. 1f, 3f or 5c with images from Taylor *et al.*, 2000, for instance). In both cases, samples show well-developed recrystallized anhydrous silicates and spinels embedded in glass. Depending on the degree of heating, the spinel rim has been more or less obliterated in experimental charges, as for most of the cosmic spherules (Genge *et al.*, 1997). This is probably partly due to an enhancement of Fe evaporation in the cosmic spherules in comparison with scoriaceous micrometeorites (Genge *et al.*, 1997), but also to a decrease in peripheral iron concentration as melting proceeds in the sample. Furthermore, both our charges and the cosmic spherules show a low vesiculation rate compared to the less heated particles (see Fig. 5c), as described by Brownlee and Bates, (1983), and Genge *et al.* (1997). The analyses performed on cosmic spherule spinels are in agreement with those obtained on our longest heated samples (run 135/1/40, Table 1). They are enriched in Mg, Al, Ni elements (2–10 wt% MgO; 2–6 wt% Al_2O_3; 1–5 wt% NiO; this study; Koeberl and Hagen, 1989; Robin *et al.*, 1992).

Scoriaceous Micrometeorites

As depicted in Fig. 9, the resemblance between a scoriaceous micrometeorite and our simulated micrometeorite (run 142/2/5; Table 1) is most convincing. In both cases, the fragments are vesiculated and show a recrystallization texture with anhydrous silicates and spinels embedded in an iron-rich partial melt, in agreement with observation of scoriaceous micrometeorites (Kurat *et al.*, 1994; Yano and Noguchi 1998; Taylor *et al.*,

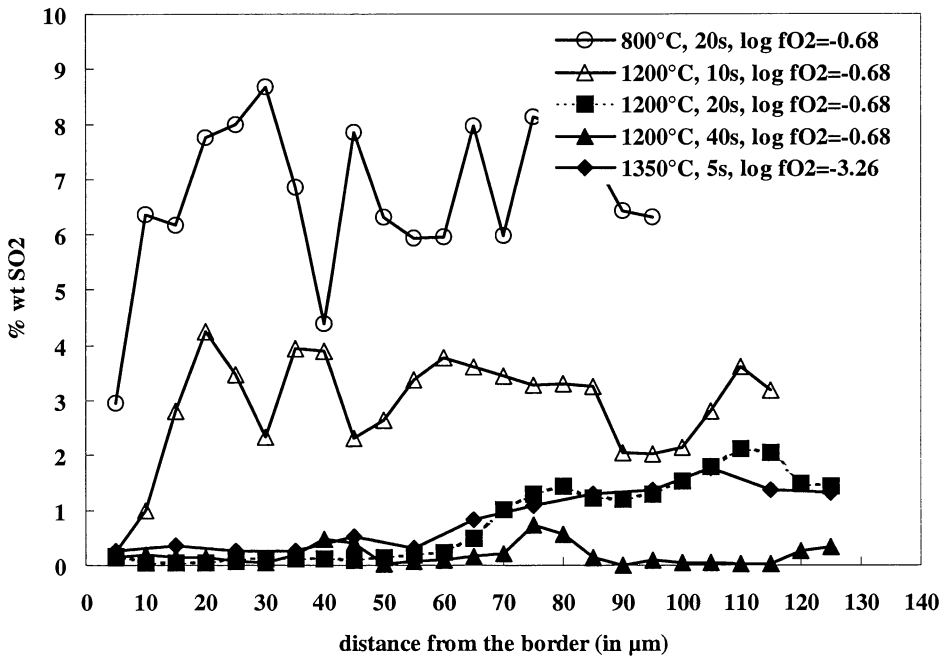

FIG. 8. Sulfur profiles (in SO_2 wt%) through Orgueil fragments for different temperatures and heating times. Note that the profile for 1350 °C was obtained for more reduced conditions ($\log fO_2 = -3.26$) and is given for comparison.

TABLE 2. Phase compositions in wt% (spinel, glass and recrystallized olivine) of heated Orgueil fragments (electron microprobe analyses) at 1350 °C under log $fO_2 = -0.68$ for different run times.*

Run no.	Time (s)	Phase	*n*	SiO_2	TiO_2	Al_2O_3	Cr_2O_3	Fe_2O_3	FeO	MnO	MgO	NiO	CaO	Na_2O	K_2O	Sum
135/1/5	5	sp.	10	0.26	0.02	0.21	0.02	70.19	17.03	0.22	8.18	0.59	–	–	–	96.72
				(0.21)	(0.03)	(0.12)	(0.03)	(1.64)	(4.26)	(0.11)	(2.78)	(0.31)				(0.65)
135/1/10	10	sp.	15	0.29	0.03	0.32	0.05	71.02	15.73	0.47	8.79	1.11	–	–	–	97.81
				(0.31)	(0.03)	(0.19)	(0.04)	(1.52)	(5.26)	(0.23)	(3.24)	(0.86)				(1.12)
135/1/20	20	sp.	17	0.35	0.04	1.04	0.05	71.35	12.25	0.29	11.12	1.44	–	–	–	97.93
				(0.29)	(0.04)	(0.36)	(0.07)	(1.12)	(2.12)	(0.07)	(1.30)	(0.38)				(0.86)
135/1/40	40	sp.	12	0.37	0.04	1.18	0.20	71.66	10.46	0.31	11.42	3.10	–	–	–	98.74
				(0.29)	(0.05)	(0.18)	(0.29)	(1.39)	(0.89)	(0.14)	(0.71)	(0.91)				(0.96)
		gl.	7	54.44	0.39	4.18	0.02	–	17.88	0.42	11.28	0.16	6.98	2.20	0.32	98.27
				(2.01)	(0.45)	(0.91)	(0.02)		(2.89)	(0.12)	(4.32)	(0.13)	(2.42)	(0.71)	(0.20)	(0.61)
		ol.	1	41.39	0.06	0.36	0.11	–	7.72	0.28	46.73	2.42	0.36	0.09	0.01	99.53

**n* represents the number of spinels analyzed in each experimental charge. Fe_2O_3, FeO are calculated by stoichiometry. Numbers in parentheses indicate one standard deviation of the analyses performed on a sample. Abbreviations: sp = spinel; gl = glass; ol = olivine.

2000). Like in our experiments, analytical TEM performed on a scoriaceous micrometeorite reveals indeed a prominent iron-enrichment of the peripheral interstitial glass up to 30 wt% FeO (47 wt% SiO_2, 14.7 wt% MgO, 6.4 wt% Al_2O_3). Both natural and simulated micrometeorites show a well-developed polycrystalline continuous spinel rim (1 to 4 μm) whose thickness is fairly independent of the nature of the substrate. Their surface aspects are also very similar (Fig. 4; Fig. 8 in Kurat *et al.*, 1994), with spinels standing out of the melt. This resemblance suggests that such external morphology of micrometeorites is not a figure of leaching of the interstitial glass during alteration by terrestrial waters but a primary texture of spinel formation. These textural similarities can be extended to the chemical compositions since the compositions of the rim spinels are very similar in both cases, varying from magnetite to magnesioferrite (this study and Robin *et al.*, 1992). However, the Fe^{3+}/Fe^{2+} ratios of our spinels (Table 2) are closer to those obtained for spinels in fusion crusts of meteorites which are decelerated at lower altitudes than micrometeorites (Robin *et al.*, 1992). This can be explained by the fact that these charges were heated in air while micrometeorites are decelerated in a more reduced atmosphere (fO_2 varying approximately between –4 to –8 log units, Robin *et al.* (1992)).

Besides these comparisons with micrometeorites, it can be noticed that there also exists a remarkable similarity of texture between these melted charges and the outer crust of some stony meteorites (Genge and Grady, 1999; Ramdohr, 1967; Fruland, 1974).

Unmelted Micrometeorites

Genge *et al.* (1997) have classified the unmelted fine-grained Antarctic micrometeorites into two textural subtypes: (1) vesicular fine-grained micrometeorites and (2) non-vesicular fine-grained micrometeorites.

Figure 10 shows the resemblance between a vesicular fine-grained micrometeorite and one of our charges (run 120/2/20, see Table 1). As described by Genge *et al.* (1997), the matrix contains abundant tiny vesicles and is dominated by an irregular homogeneous phase, product of the thermal decomposition of the phyllosilicates. The spinel rim on fine-grained micrometeorites is a very fine-grained (0.5 to 1 μm thick) rim, sometimes discontinuous, and is less developed than on scoriaceous micrometeorites (~1–4 μm thick) (Kurat *et al.*, 1994; Genge *et al.*, 1997). Clusters of spherical or framboidal magnetites are sometimes still present in the charges (Fig. 2c) as for the unmelted micrometeorites (Fig. 10c) (Kurat *et al.*, 1992).

It is more difficult to reproduce the non-vesicular fine-grained micrometeorites. Hence, in the least heated of our charges (Table 1, runs 1200/1/5, 1200/1/10, and Fig. 2a,b), the matrix is thermally destabilized showing numerous dehydration cracks, whereas texture of the non-vesicular fine-grained micrometeorites does not give evidence for thermal modification. Furthermore, the simulated micrometeorites do not show any fine-grained spinel rim such as for the non-vesicular fine-grained micrometeorites but a very thin discontinuous iron-rich rim. The difficulty to reproduce such type of micrometeorites could be explained either because the experimental techniques do not allow simulation of pulse-heating over times shorter than 2 s or because in the experiments, heating occurs by radiation and conduction rather than by hypervelocity impact of air molecules.

Several authors (*e.g.*, Kurat *et al.*, 1994; Genge *et al.*, 1997), reported the occurrence of an unmelted core in scoriaceous micrometeorites, suggesting that a very high thermal gradient

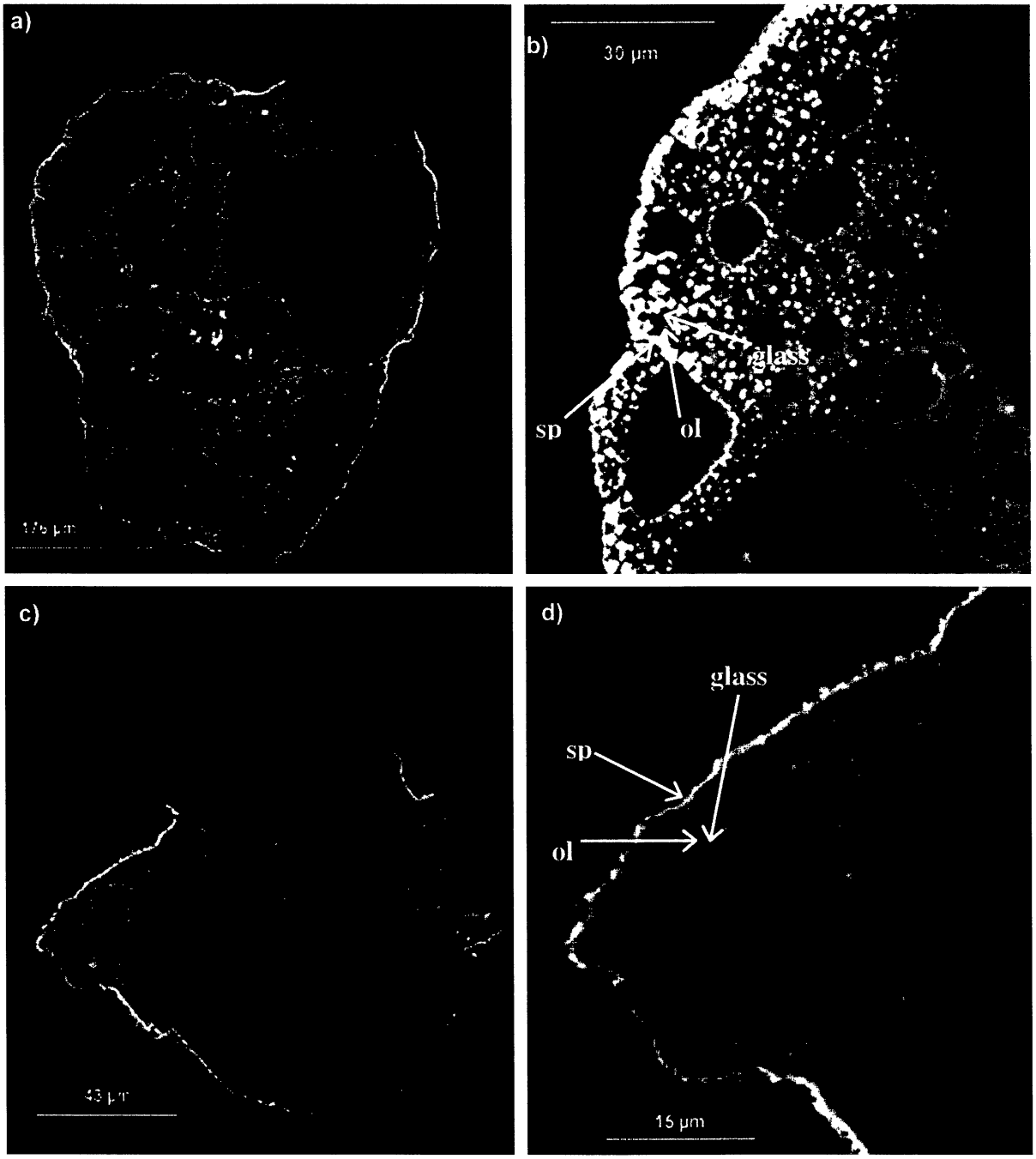

FIG. 9. Comparison between backscattered electron images of polished sections of one experimental charge (run 142/2/5, Table 1) (a, b), and of a scoriaceous micrometeorite (c, d).

between the surface and the interior of the micrometeorites could exist. To explain the presence of such thermal heterogeneity, Szydlik and Flynn (1992) calculated the interior temperature of a particle using an homogeneous thermal diffusivity through the particle. They showed that mechanisms such as local phase transformations of phyllosilicates are then necessary to produce the observed thermal gradient. Bonny and Balageas (1990) suggested that pyrolysis of carbonaceous material could prevent micrometeorites from reaching a high temperature by endothermic reactions, but could not reproduce such a high thermal gradient inside a particle of ~100 μm. Genge and Grady (2000) proposed that the higher temperature of the surface could act to reduce the temperature increase inside

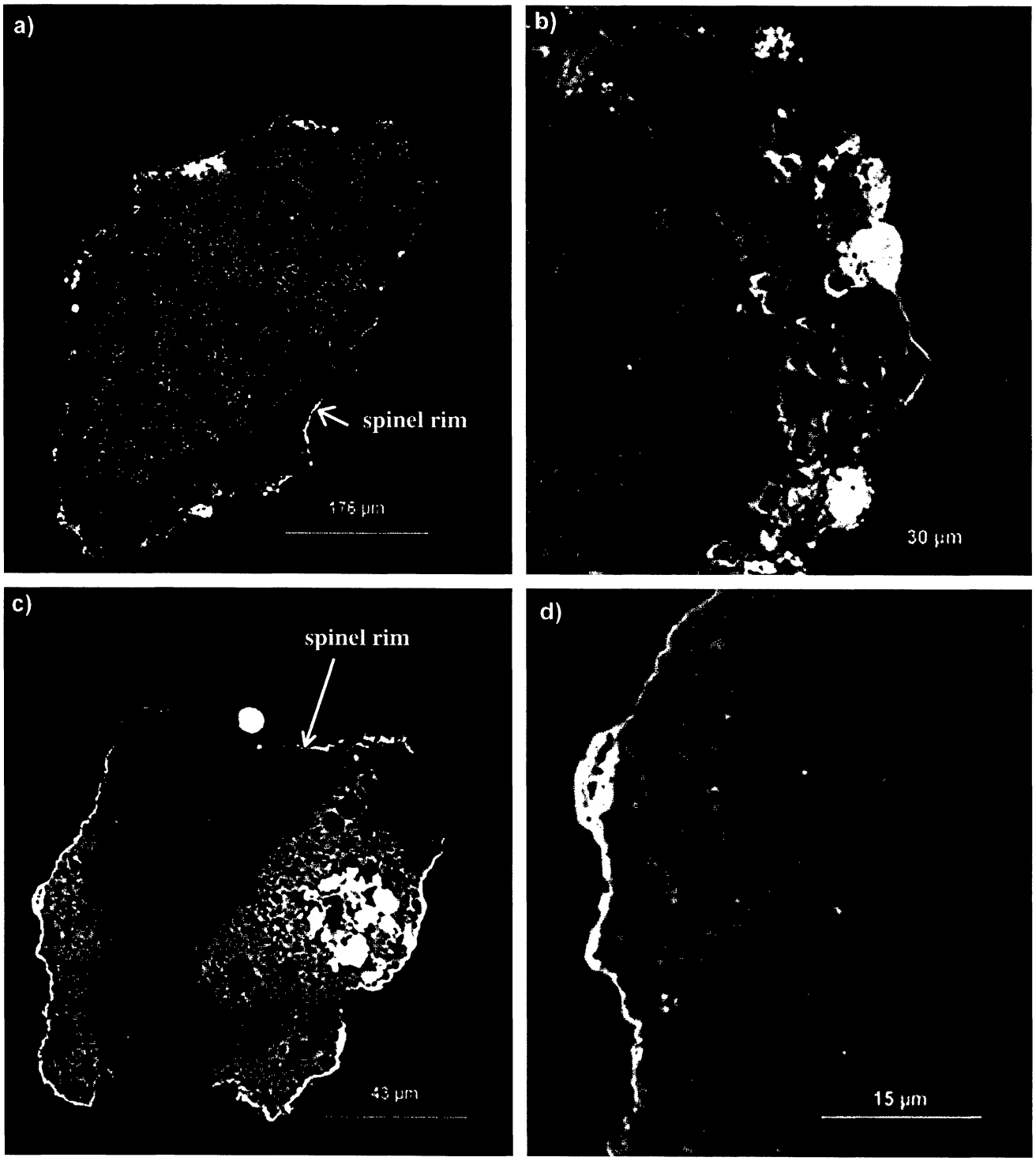

FIG. 10. Comparison between backscattered electron images of polished sections of experimental charges (run 120/2/20; 120/1/20, Table 1) (a, b) and of a vesicular fine-grained micrometeorite (c, d).

the micrometeorites thanks to an efficient evaporation and radiation mechanisms. They showed that the thermal gradient between the surface and the core of the particle could exceed 600 °C. Our present observations showing thermally destabilized phyllosilicate cores with a melted borders confirm the possibility of such temperature gradients inside the particles.

Pulse-heating experiments reproduce most of the effects of heating observed on micrometeorites depending on the temperature, run time and oxygen fugacity. Furthermore, since the spinel rim observed on the micrometeorites is experimentally reproduced under controlled conditions, it will allow us to better understand its formation using our textural, mineralogical and chemical results.

MECHANISMS OF THE SPINEL RIM FORMATION

Scenarios have already been proposed to explain the formation of the spinel rim. Several authors (Jessberger *et al.*, 1992; Kurat *et al.*, 1994; Maurette, 1998) suggested that it could be formed by accretion or condensation of Fe from the iron-rich layer E (80 km) of the atmosphere (Steinweg *et al.*, 1992). The origin of this Fe-enrichment is generally attributed to the ablation of meteorites and micrometeorites at this altitude (Kane and Gardner, 1993). However, because of the low column density of Fe measured in the layer E, it is unlikely that an accretion occurring during a few seconds can produce a 1 μm thick spinel rim (Flynn, 1994). Furthermore, recent studies of micrometeorites (Genge *et al.*, 1997) have shown that the spinel rim is more developed on scoriaceous micrometeorites than on unmelted micrometeorites, which argues against a formation by an accretionary process. Kurat *et al.* (1994) has suggested that the Mg, Al, Ni and Si enrichments of the spinels support an origin of the shell by condensation. We think that this putative Si enrichment is principally due to a secondary fluorescence phenomena during the electron microprobe analyses. Furthermore, an enrichment of Mg and Al by the vapor phase should lead to a roughly constant concentration of these elements in the spinels of micrometeorites shell. However, variations in the concentration of these elements in the spinels argue against this idea exposed by Kurat *et al.* (1994).

In IDPs, Keller *et al.* (1996) proposed a formation of the spinel rim through sub-solidus mineral reactions activated by the heating, such as oxidation of Fe from iron-rich phases (Fe-Ni sulfide, olivine, phyllosilicate). For the scoriaceous and vesicular fine-grained micrometeorites, evidence for peripheral partial melting (Genge *et al.*, 1997; Yano and Noguchi, 1998) may imply a formation of the spinel rim through sub-liquidus reactions.

In contrast with previous scenarios, our detailed experimental study allows us to propose a new scenario for the micrometeorite spinel rim formation.

Observations at 1200 °C for short run times support the idea that the iron-rich phases of micrometeorites such as ferrihydrite are first thermally destabilized leading to larger iron-rich domains due to crystallization of minute iron oxides (*e.g.*, Cornell and Schwertmann, 1996). These iron-rich domains are more numerous along the cracks and along the periphery of the fragment due to a preferential dehydration at these places. A very fine iron-rich discontinuous rim could then form around the sample by sub-solidus reactions, as observed on the less heated micrometeorites.

Observations at 1350 °C or at 1200 °C for longer run times, such as the presence of small euhedral spinel crystals embedded in glass (*e.g.*, Fig. 9b), suggest that this iron-rich phases destabilization is rapidly accompanied by a peripheral partial melting linked to a very high thermal gradient at the periphery of the sample. We can assume that the first phases to melt are the Fe^{3+}-rich ferrihydrite (Tomeoka and Buseck, 1988) and the phyllosilicates leading to a silicate melt highly rich in iron. Due to its low saturation level, spinel is oversaturated in the melt favoring at first high nucleation rates (Muan and Osborn, 1956). Consequently, spinels crystallizing during short pulse-heating (Fig. 4a) are small and numerous whereas they become larger and less abundant as the duration of the pulse increases (Fig. 4b). The crystallization of a continuous spinel rim, independent of the nature of the substrate, suggests that the Fe-rich silicate melt wets the whole sample surface. This is observable on the scoriaceous micrometeorites (*e.g.*, Fig. 8d in Kurat *et al.*, 1994). The melt evolves from an iron-rich composition to a more Si-, Mg-, Al-rich composition as melting progresses inward, leading to concomitant changes in the spinel composition (Mg and Al contents). For short pulse-heating, the spinel composition is very sensitive to the local composition of the melt whereas for longer duration, its composition is buffered by a more homogeneous melt obtained at higher partial melting rates.

With the increase of the pulse-heating duration, the peripheral partial melting spreads toward the core of the sample leading to the progressive crystallization of idiomorphous spinels inside the fragment together with pyroxenes and olivines. This ubiquitous spinel crystallization within the fragment leads to the obliteration of the spinel rim. For higher temperatures with elevated partial melting rates, this scenario predicts the total loss of the spinel rim, as observed on some cosmic spherules.

IMPLICATIONS

Elemental Depletions–Large depletions of S, Ca and Ni with respect to the chondritic composition have been observed in many partially melted micrometeorites (*e.g.*, Kurat *et al.*, 1994; Engrand and Maurette, 1998). Assuming that the particles initially have a primitive chondritic composition, authors have explained these depletions by aqueous alteration of soluble salts in the ice (Maurette *et al.*, 1992; Kurat *et al.*, 1994) or by volatilization during the atmospheric entry (*e.g.*, Fraundorf *et al.*, 1982). Figure 7 shows that our experimental charges are only depleted in sulfur relative to CI chondrite and do not show any Ni or Ca depletion. This supports the idea that the Ca and Ni depletions are probably due to terrestrial alteration whereas the one of S is principally due to its volatilization during the atmospheric entry (*e.g.*, Greenwood and Hutchison, 1993).

The S depletion during the atmospheric entry is related to the degree of heating suffered by the micrometeorite precursor, that is, to the temperature and the duration at the peak temperature. It may also be related to the oxygen fugacity. However, variations in bulk S content are likely to occur due to primary heterogeneity. Hence, it seems more relevant to use the S content profile through a particle as a pulse-heating conditions indicator rather than the absolute S bulk composition. Other studies on IDPs and micrometeorites have also demonstrated the absence of correlation between the bulk sulfur content and other indicators of entry heating (*e.g.*, Flynn *et al.*, 1993a; Osawa *et al.*, 2000).

Conditions of Atmospheric Entry of Micrometeorites– Cometary particles are generally more heated than asteroidal particles of the same size and mass, for similar entry angles (Love and Brownlee, 1991) because of their higher entry velocities. It should thus be possible to constrain the origin of the extraterrestrial dust particles according to the degree of heating they experienced during their deceleration (Flynn, 1989; Jackson and Zook, 1992). For instance, for IDPs, several thermometers have already been proposed to quantify this degree of heating. Based on experimental results, Flynn (1989) used the volatile contents of heated IDPs to constrain the peak temperature they suffer. Other studies on IDPs have been performed using the He depletion (Nier and Schlutter, 1992; Brownlee and Joswiak, 1995), the solar flare occurrence (*e.g.*, Sandford, 1986; Fraundorf *et al.*, 1982), or the mineralogy and the spinel rim occurrence (*e.g.*, Keller *et al.*, 1996; Flynn, 1994; Rietmeijer, 1996).

In a similar way, our experimental results suggest that the texture and mineralogy of micrometeorites can be used as a thermometer. Spinel rim development, the degree of recrystallization and vesiculation allow the peak temperature and the duration of the heating for micrometeorites to be estimated. Assuming that a pulse-heating duration is less than 20 s, the features of the heated Orgueil fragments analogue to micrometeorites allow us to limit fields representing the different types of micrometeorites as a function of temperature and duration of the pulse-heating (Fig. 11) into (1) the non-vesicular fine-grained micrometeorites, (2) the vesicular fine-grained micrometeorites, (3) the scoriaceous micrometeorites and (4) the cosmic spherules. Due to our experimental choices (Orgueil as starting material, number of experiments, influence of the fO_2), uncertainties still remain, notably on the extension of the non-vesicular fine-grained field as well as on the field boundaries for short duration heating-pulses (<2 s). Despite these restrictions, this model allows the peak temperature and the duration of the heating to be estimated for large micrometeorites (200–400 μm) from their texture and their mineralogical composition. It indicates the restrictive conditions of temperature and time necessary for the apparition of the spinel rim.

As previously outlined, there exists a discrepancy between the large proportions of melted to unmelted micrometeorites predicted by the theoretical atmospheric entry models (*e.g.*, Love and Brownlee, 1991) and those which are observed, for instance, at Cap-Prudhomme, Antarctica (Engrand and Maurette, 1998). In general, these models determine the melting rate of a particle at equilibrium conditions and for a given composition. For instance, in the model of Love and Brownlee (1991), all particles heated above 1350 °C are considered to be at least 50% melted (*i.e.*, to be cosmic spherules). However, our data (Fig. 11) show clearly that at a given temperature, the melting rate of a particle is strongly dependant on the duration

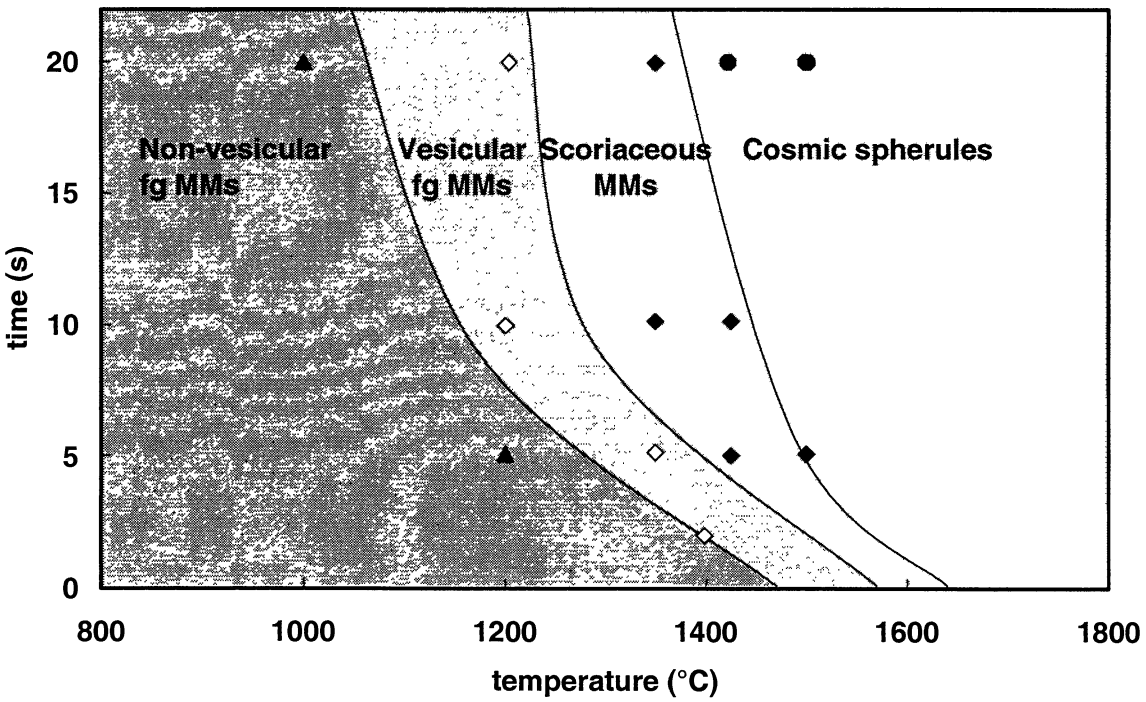

FIG. 11. Conditions of heating suffered by large micrometeorites (200–400 μm) during atmospheric entry deduced from their texture and mineralogy. The different symbols reported in the graph represent the experimental charges: filled triangle (field "non-vesicular fine-grained micrometeorites") indicates samples showing only minor dehydration without spinel rim or vesiculation. Open diamond (field "vesicular fine-grained micrometeorites) indicates samples showing a slight vesiculation and a thin spinel rim. Filled diamond (field "scoriaceous micrometeorites") indicates samples showing evidence for partial-melting progressing inward, well-developed vesiculation and a thick spinel rim. Filled octagon (field "cosmic spherules") indicates completely melted samples with no vesiculation and without spinel rim.

of the heating pulse, and generally inferior to the one obtained at equilibrium conditions. This may therefore explain why models systematically overestimate the proportions of melted particles. Our study thus shows that the kinetic processes occurring during the heating can not be neglected to determine the proportions of the different types of micrometeorites.

CONCLUSIONS

The pulse-heating experiments, presented herein to simulate the atmospheric entry of micrometeorites, reproduce both most of the heating effects observed on micrometeorites and the different types of micrometeorites, that is, (1) the fine-grained particles slightly loaded with tiny vesicles and encapsulated by a very thin, sometimes discontinuous, spinel rim (fine-grained micrometeorites); (2) the highly vesicular particles constituted by anhydrous silicates embedded in melt and surrounding by a well-developed continuous spinel rim (scoriaceous micrometeorites); and (3) the completely melted particles showing large spinels and anhydrous silicates without vesiculation nor spinel rim (cosmic spherules). In view of the similarities between our charges and micrometeorites, it is clear that the spinel rims observed on most micrometeorites form by the mechanism effective in our experiments. Thus, the polycrystalline continuous spinel rim occurrence on micrometeorites depends on temperature, duration and oxygen fugacity. Its formation implies a peripheral partial melting of iron-rich phases due to an elevated radial thermal gradient inside the particle with subsequent crystallization of the spinel crystals from an iron-rich melt. Spinel rim formation on the less heated micrometeorites may imply thermal destabilization of iron-rich phases leading to the formation of a very thin discontinuous iron-rich rim by sub-solidus reactions.

This experimental study has allowed the conditions of micrometeorites atmospheric entry such as the peak temperature and the duration of the heating-pulse to be constrained, which could be useful for determining their asteroidal or cometary origin. In addition, variations in composition of the recrystallized spinels may allow the atmospheric entry conditions of micrometeorites to be identified even more accurately (Toppani and Libourel, unpub. data).

Acknowledgements–A. Rouillier is thanked for assistance in the high-temperature experimental laboratory of the CRPG-CNRS. We also thank G. Matrajt and M. Gounelle for help with preparation and handling of the samples and for fruitful discussions. We are also grateful to A. Köhler, R. Podor, F. Diot, S. Barda for assistance for electron microprobe analyses and SEM at the Service d'Analyses of the Université Henri Poincaré, Nancy (France). Meteorite samples were kindly provided by G. Matrajt at CSNSM in Orsay and by F. Robert from the Museum National d'Histoire Naturelle de Paris. The authors are grateful to D. E. Brownlee, M. J. Genge and F. J. M. Rietmeijer for their thorough and helpful review. This work was supported by PNP (G. L.) in CRPG-CNRS and by IN2P3 and CNES in CSNSM, Orsay. This is a CRPG contribution no. 1529.

Editorial handling: D. E. Brownlee

REFERENCES

BARBER D. J. (1981) Matrix phyllosilicates and associated minerals in C2M carbonaceous chondrites. *Geochim. Cosmochim. Acta* **45**, 945–970.

BEATTIE P., FORD C. AND RUSSEL D. (1991) Partition coefficients for olivine-melt and orthopyroxene-melt system. *Contrib. Mineral. Petrol.* **109**, 212–224.

BLANCHARD M. B. (1972) Artificial meteor ablation studies: Iron oxides. *Geophys. Res. Lett.* **77**, 2442–2455.

BLANCHARD M. B. AND CUNNINGHAM G. G. (1974) Artificial meteor ablation studies: Olivine. *Geophys. Res. Lett.* **79**, 3973–3980.

BLANCHARD M. B. AND DAVIS A. S. (1978) Analysis of ablation debris from natural and artificial iron meteorites. *Geophys. Res. Lett.* **83**, 1793–1808.

BONNY P. AND BALAGEAS D. (1990) Entry corridor of micrometeorites containing organic material (abstract). *Lunar Planet. Sci.* **21**, 111–112.

BÖSTROM K. AND FREDRIKSSON K. (1966) Surface conditions of the Orgueil meteorite parent body as indicated by mineral associations. *Smithsonian Misc. Coll.* **151**, 1–39.

BROOKS C. K., LARSEN L. M. AND NIELSEN T. F. D. (1991) Importance of iron-rich tholeiitic magmas at divergent plate margins: A reppraisal. *Geology* **19**, 269–272.

BROWNLEE D. E. (1985) Cosmic dust: Collection and research. *Ann. Rev. Earth Planet. Sci.* **13**, 147–173.

BROWNLEE D. E. AND BATES B. (1983) Meteor ablation spherules as chondrule analogs. In *Chondrules and their Origins* (ed. E. A. King), pp. 10–25. Lunar and Planetary Institute, Houston, Texas, USA.

BROWNLEE D. E. AND JOSWIAK D. J. (1995) Identification of individual cometary IDP's by thermally stepped He release (abstract). *Lunar Planet. Sci.* **26**, 183–184.

CHRISTOPHE MICHEL-LEVY M. AND BOUROT-DENISE M. (1992) Mineral composition in Antarctic and Greenland micrometeorites. *Meteoritics* **27**, 73–80.

CORNELL R. M. AND SCHWERTMANN U. (1996) *The Iron Oxides. Structures, Properties, Reactions, Occurrence and Uses.* VCH, Weinheim, Germany. 573 pp.

CORRIGAN G. AND GIBB F. G. F. (1979) The loss of Fe and Na from a basaltic melt during experiments using the wire-loop method. *Mineral. Mag.* **43**, 121–126.

ENGRAND C. AND MAURETTE M. (1998) Carbonaceous micrometeorites from Antarctica. *Meteorit. Planet. Sci.* **33**, 565–580.

FLYNN G. J. (1989) Atmospheric entry heating: A criterion to distinguish between asteroidal and cometary sources of interplanetary dust. *Icarus* **77**, 287–310.

FLYNN G. J. (1994) Changes to the composition and mineralogy of interplanetary dust particles by terrestrial encounters. In *Analysis of Interplanetary Dust* (eds. M. E. Zolensky, T. L. Wilson, F. J. M. Rietmeijer and G. J. Flynn), pp. 127–143. American Institute of Physics, Woodbury, New York, USA.

FLYNN G. J., SUTTON S. R., BAJT S., KLÖCK W., THOMAS K. L. AND KELLER L. P. (1993a) Depletions of sulfur and/or zinc in IDPs: Are they reliable indicators of atmospheric entry heating? (abstract). *Lunar Planet. Sci.* **24**, 497–498.

FLYNN G. J., SUTTON S. R. AND KLÖCK W. (1993b) Compositions and mineralogies of unmelted polar micrometeorites: Similarities and differences with IDPs and meteorites. *Proc. NIPR Symp. Antarct. Meteorites* **6**, 304–324.

FOLINSBEE K., DOUGLAS J. A. V. AND MAXWELL J. A. (1967) Revelstoke, a new type I carbonaceous chondrite. *Geochim. Cosmochim. Acta* **31**, 1625–1635.

FRAUNDORF P. (1980) The distribution of temperature maxima for micrometeorites decelerated in the Earth's atmosphere without melting. *Geophys. Res. Lett.* **10**, 765–768.

FRAUNDORF P., LYONS T. AND SCHUBERT P. (1982) The survival of solar flare tracks in interplanetary dust silicates on deceleration in the Earth's atmosphere. *J. Geophys. Res.* **87**, A409–A412.

FRULAND R. M. (1974) Fusion crust phenomena on some carbonaceous chondrites. *Meteoritics* **9**, 339–342.

FUCHS L. H., OLSEN E. AND JENSEN K. J. (1973) Mineralogy, mineral-chemistry and composition of the Murchison (C2) meteorite. *Smithsonian Contr. Earth Sci.* **10**, 1–39.

GENGE M. J. AND GRADY M. M. (1999) The fusion crusts of stony meteorites: Implications for the atmospheric reprocessing of extraterrestrial materials. *Meteorit. Planet. Sci.* **34**, 341–356.

GENGE M. J. AND GRADY M. M. (2000) The thermal evolution of micrometeroids during atmospheric entry (abstract). *Lunar Planet. Sci.* **31**, 1361–1362.

GENGE M. J., GRADY M. M. AND HUTCHISON R. (1997) The textures and compositions of fine-grained Antarctic micrometeorites: Implications for comparisons with meteorites. *Geochim. Cosmochim. Acta* **61**, 5149–5162.

GOUNELLE M. (2000) Matière extraterrestre sur Terre: des Océans aux protoétoiles. Ph.D. Thesis. Université Paris 7, Denis Diderot, Paris, France. 171 pp.

GREENWOOD R. C. AND HUTCHISON R. (1993) Atmospheric entry heating of macro- and micrometeorites: A comparative study. *Meteoritics* **28**, 356–357.

GRESHAKE A., KLÖCK W., ARNDT P., MAETZ M., FLYNN G. J., BAJT S. AND BISCHOFF A. (1998) Heating experiments simulating atmospheric entry heating of micrometeorites. Clues to their parent body sources. *Meteorit. Planet. Sci.* **33**, 267–290.

GROVE T. L. (1981) Use of FePt alloys to eliminate the iron loss problem in 1 atmosphere gas mixing experiments: Theoretical and practical considerations. *Contrib. Mineral. Petrol.* **78**, 298–304.

HAGGERTY S. E. (1976) Opaque mineral oxides in terrestrial igneous rocks. In *Oxide Minerals* (ed. D. Rumble), pp. 101–300. Mineralogical Society of America, Washington, D.C., USA.

HUA X. AND BUSECK P. B. (1998) Unusual forms of magnetite in the Orgueil carbonaceous chondrite (abstract). *Meteorit. Planet. Sci.* **33 (Suppl.)**, A215–A220.

HUGHES D. H. (1978) Meteors. In *Cosmic Dust* (ed. J. A. M. McDonnel), pp. 123–185. Wiley, New York, New York, USA.

HYMAN M. AND ROWE M. W. (1983) Magnetites in CI chondrites (abstract). *Lunar Planet. Sci.* **13**, A736–A740.

HYMAN M., ROWE M. W. AND HERNDON J. M. (1978) Magnetite heterogeneity among CI chondrites. *Geochem. J.* **13**, 37–39.

JACKSON A. A. AND ZOOK H. A. (1992) Orbital evolution of dust particles from comets and asteroids. *Icarus* **97**, 70–84.

JAROSEWICH E. (1990) Chemical analyses of meteorites: A compilation of stony and iron meteorite analyses. *Meteoritics* **25**, 323–337.

JEDWAB J. (1965) Structures framboïdales dans la météorites d'Orgueil. *C. R. Acad. Sci. (Paris)* **261**, 2923–2925.

JEDWAB J. (1971) La magnétite de la météorite d'Orgueil vue au microscope électronique à balayage. *Icarus* **35**, 319–340.

JESSBERGER E. K., BOHSUNG J., CHAKAVEH S. AND TRAXEL K. (1992) The volatile element enrichment of chondritic interplanetary dust particles. *Earth Planet. Sci. Lett.* **112**, 91–99.

KANE T. J. AND GARDNER C. S. (1993) Lidar observations of the meteoric deposition of mesospheric metals. *Science* **259**, 1297–1299.

KELLER L. P., THOMAS K. L. AND MCKAY D. S. (1996) Mineralogical changes in IDPs resulting from atmospheric entry heating. In *Physics, Chemistry, and Dynamics of Interplanetary Dust—Proceedings of the 150th Colloquium of the International Astronomical Union* (eds. B. A. S. Gustafson and M. S. Hanner), pp. 295–298. Astronomical Society of the Pacific Conferences Series, Gainesville, Florida, USA.

KERRIDGE J. F. (1970) Some observations on the nature of magnetite in the Orgueil meteorite. *Earth Planet. Sci. Lett.* **9**, 299–306.

KOEBERL C. AND HAGEN E. H. (1989) Extraterrestrial spherules in glacial sediment from Transantarctic Mountains, Antarctica: Structure, mineralogy, and chemical composition. *Geochim. Cosmochim. Acta* **53**, 937–944.

KURAT G., PRESPER T. AND BRANDSTÄTTER F. (1992) CI-Like micrometeorites from Cap Prudhomme, Antarctica (abstract). *Lunar Planet. Sci.* **23**, 747–748.

KURAT G., KOEBERL C., PRESPER T., BRANDSTÄTTER F. AND MAURETTE M. (1994) Petrology and geochemistry of Antarctic micrometeorites. *Geochim. Cosmochim. Acta* **58**, 3879–3904.

LOVE S. G. AND BROWNLEE D. E. (1991) Heating and thermal transformation of micrometeoroids entering the Earth's atmosphere. *Icarus* **89**, 26–43.

LOVE S. G. AND BROWNLEE D. E. (1993) A direct measurement of the terrestrial mass accretion rate of cosmic dust. *Science* **262**, 550–553.

MAURETTE M. (1998) Carbonaceous micrometeorites and the origin of life. *Orig. Life and Evol. Biosphere* **28**, 385–412.

MAURETTE M., HAMMER C., BROWNLEE D. E., REEH N. AND THOMSEN H. H. (1986) Placers of cosmic dust in the blue ice lakes of Greenland. *Science* **233**, 869–872.

MAURETTE M., BONNY P., BRACK A., JOURET C., POURCHET M. AND SIRY P. (1991a) Carbon-rich micrometeorites and prebiotic synthesis. In *Bioastronomy: The Search for Extraterrestrial Life* (eds. J. Heidmann and M. J. Klein), pp. 124–132. Springer-Verlag, Berlin, Germany.

MAURETTE M., OLINGER C., CHRISTOPHE MICHEL-LEVY M., KURAT G., POURCHER M., BRANDSTÄTTER F. AND BOUROT-DENISE M. (1991b) A collection of diverse micrometeorites recovered from 100 tonnes of Antarctic blue ice. *Nature* **351**, 44–47.

MAURETTE M., KURAT G., PRESPER T., BRANDSTÄTTER F. AND PERREAU M. (1992) Possible causes of depletion and enrichment of minor elements in Antarctic micrometeorites (abstract). *Lunar Planet. Sci.* **23**, 861–862.

MCSWEEN H. Y., JR. AND RICHARDSON S. M. (1977) The composition of carbonaceous chondrite matrix. *Geochim. Cosmochim. Acta* **41**, 1145–1161.

MUAN A. AND OSBORN E. F. (1956) Phase equilibria at liquidus temperatures in the system MgO-FeO-Fe_2O_3-SiO_2. *J. Am. Ceramic Soc.* **39**, 121–140.

NAGY B. AND CLAUS G. (1962) Notes on the petrography of the Orgueil meteorite. In *Advances in Organic Geochemistry* (eds. U. Colombon and G. D. Hobson), pp. 115–118. Pergamon Press, New York, New York, USA.

NIELSEN R. L., FORSYTHE L. M., GALLAHAN W. E. AND FISK M. R. (1994) Major- and trace-element magnetite-melt equilibria. *Chem. Geol.* **117**, 167–191.

NIER A. O. AND SCHLUTTER D. J. (1992) Extraction of helium from individual interplanetary dust particles by step-heating. *Meteoritics* **27**, 166–173.

NOGUCHI T. AND NAKAMURA T. (2001) Mineralogy of phyllosilicate-rich micrometeorites and comparison with Tagish Lake CI and Sayama CM chondrites (abstract). *Lunar Planet. Sci.* **32**, #1541, Lunar and Planetary Institute, Houston, Texas, USA (CD-ROM).

OSAWA T., NAGAO K., NAKAMURA T. AND TAKAOKA N. (2000) Noble gas measurement in individual micrometeorites using laser gas-extraction system. *Antarctic Met. Res.* **13**, 322–341.

POPOVA O. P., SIDNEVA S. N., SHUVALOV V. V. AND STRELKOV A. S. (2000) Screening of meteoroids by ablation vapor in high-velocity meteors. *Earth, Moon Planets* **82-83**, 109–128.

RAMDOHR P. (1967) Die schmelzkruste der meteoriten. *Earth Planet. Sci. Lett.* **2**, 197–209.

RIETMEIJER F. J. M. (1996) Cellular precipitates of iron oxide in olivine in a stratospheric interplanetary dust particle. *Mineral. Mag.* **60**, 877–885.

RIETMEIJER F. J. M. AND NUTH J. A., III (2000) Collected extraterrestrial materials: Constraints on meteor and fireball compositions. *Earth, Moon Planets* **82-83**, 325–350.

ROBIN E., BONTÉ P., FROGET L., JÉHANNO C. AND ROCCHIA R. (1992) Formation of spinels in cosmic objects during atmospheric entry: A clue to the Cretaceous–Tertiary event. *Earth Planet. Sci. Lett.* **108**, 181–190.

SANDFORD S. A. (1986) Solar flare track densities in interplanetary dust particles: The determination of an asteroidal *versus* cometary source of the zodiacal dust cloud. *Icarus* **68**, 377–394.

SANDFORD S. A. AND BRADLEY J. P. (1989) Interplanetary dust particles collected in the stratosphere: Observations of atmospheric heating and constraints on their interrelationships and sources. *Icarus* **82**, 146–166.

STEINWEG A., KRANKOWSLI D. AND LÄMMERZAHL B. (1992) Metal ions layers in the auroral E-region measured by mass spectrometers. *J. Atmos. Terr. Phys.* **54**, 703–714.

SZYDLIK P. P. AND FLYNN G. J. (1992) The internal temperature profiles of large micrometeorites during atmospheric entry (abstract). *Meteoritics* **27**, 294–295.

TAYLOR S., LEVER J. H. AND HARVEY R. P. (2000) Numbers, types, and compositions of an unbiased collection of cosmic spherules. *Meteorit. Planet. Sci.* **35**, 651–666.

TOMEOKA K. AND BUSECK P. R. (1988) Matrix mineralogy of the Orgueil CI carbonaceous chondrite. *Geochim. Cosmochim. Acta* **52**, 1627–1640.

WHIPPLE F. L. (1951) The theory of micrometeorites, 2. In a heterothermal atmosphere. *Proc. Nat. Acad. Sci.* **37**, 19–30.

YADA T. AND KOJIMA H. (2000) The collection of micrometeorites in the Yamato meteorite ice field of Antarctica in 1998. *Antarctic Met. Res.* **13**, 9–18.

YANO H. AND NOGUCHI T. (1998) Sample processing and initial analysis techniques for Antarctic meteorites. *Antarctic Met. Res.* **11**, 136–154.